

## NUMERICAL SIMULATION OF ION TRANSPORT DURING ANODIC BONDING

**Mauricio Fabbri**

**José Roberto Sbragia Senna**

*fabbri@las.inpe.br*

*jrsenna@las.inpe.br*

Laboratório Associado de Sensores e Materiais - LAS

Instituto Nacional de Pesquisas Espaciais

CP 515, 12.201-970 São José dos Campos – SP – Brazil

**Abstract.** *We describe a stable numeric discretization procedure of the ionic non-linear transport equations that governs the depletion layer dynamics during electrostatic bonding, in the absence of carrier diffusion. The numerical scheme allows for independent cation and anion mobility models, and can be accommodated to handle more complicated effects, such as the oxide layer build-up at the metal-glass interface and the interdependence between sodium and oxygen transport. For Pyrex-on-silicon (s-g) bonding, results from our simulations show that the correct global transient behavior is achieved when the oxygen mobility in the glass is around one-fifth of the value for the sodium ions; under those conditions, the depletion-layer charge profiles are rather concentrated around the depletion front (away from the s-g interface), yielding an essentially neutral depletion zone almost everywhere. Consideration of an additional potential drop due to oxide electrochemical deposition at the bonding interface does not change qualitatively the model predictions.*

**Keywords:** *anodic bonding, electrostatic bonding, electric depletion layer, moving boundary problems*

## 1. INTRODUCTION

Anodic bonding is an important usual technique in microfabrication for metal-glass sealing, and was introduced by Wallis and Pomeranz in 1969. Typically, a metal-insulator junction is made by clean mechanical contact between a sodium containing glass plate and a metal or semiconductor. The junction is then heated around 300°C and a high constant voltage (~1000V) is applied between the metal (anode) and the glass (cathode) – a metal contact being provided to the free glass surface. At those moderated high temperatures, sodium cations  $\text{Na}^+$  from the dissociation of  $\text{Na}_2\text{O}$  inside the glass migrate towards the cathode. Since the dissociated oxygen anions have a small mobility (and the temperature is still too low for any significant electronic conduction), a depletion layer is formed in the glass, in the vicinity of the glass-metal interface. The high electrostatic field brings the surfaces into intimate contact, and metal oxide is then formed at the interface (it is believed that the source of oxygen atoms is the natural humidity present in the glass). That provides a clear and homogeneous welding which conforms to large contact areas and allow bonding between surfaces that are not perfectly planar - for that reason it has been intensively used for cavity sealing and device encapsulation. In practice, usually a large bonding surface (around  $100\text{cm}^2$ ) is first assembled, submitted to the bonding process and then cut into final units.

The behavior of the transient electric current during the bonding process provides indirect information about the electric transport inside the glass and the dynamics of the depletion layer build-up. It is clearly observed distinct short-term and long-range regimes, which have been modeled either by equivalent-circuit models (Anthony, 1983; Albaugh, 1991) or by microscopic mean-field ohmic transport (Carlson et al., 1972; Rios et al., 2000). In the improved model by Rios et al. (2000), a critical field value is introduced, above which oxygen transport is allowed through the glass, thus providing a threshold for distinct short and long-term behavior. Nevertheless, all of those models so far have failed to account for the global observed electrical transient, as they predict either a too-short initial regime or an incorrect long-range behavior.

The correct picture of charge transfer inside the depletion layer requires a detailed charge-compensation mechanism that has not been adequately taken into account by earlier works, which aimed at models with analytic closed solutions. In this work, we describe a numerical scheme that allows for independent sodium and oxygen mobility models, and considers the interdependence between sodium and oxygen transport. Results then show that the correct global transient behavior seems to be achieved when the oxygen anions mobility is enough to yield an essentially neutral depletion zone almost everywhere, with a rather concentrated charge profile around the depletion front (away from the glass-metal interface). Oxygen mobility is thus likely to set up anion transport into the glass at very early stages of the bonding process.

Nevertheless, important detailed discrepancies still remain between the numerical simulations and the known experimental behavior of the electric transient. We thus investigate the issue further by taking into account the insulating oxide layer build-up at the silicon-glass interface.

## 2. ELECTROSTATIC MODEL FOR THE DEPLETION-LAYER BUILD-UP

We denote the normalized sodium (cation) and oxygen (anion) charge densities inside the glass by  $\rho_+$  and  $\rho_-$ , respectively, such that  $0 \leq \rho_{+,-} \leq 1$  ( $\rho_{+,-} = n_{+,-}/n_{0+}$ , where  $n_{0+}$  is the initial sodium content in the glass). Initially (time  $t=0$ ) the glass is uniformly neutral,  $\rho_+ = \rho_-$ , the net charge  $\rho = \rho_+ - \rho_-$  is zero and the electric field  $E = E_0$  is uniform throughout. Then sodium cations  $\text{Na}^+$ , from the dissociation of  $\text{Na}_2\text{O}$  inside the glass, begin to be dragged by

the electric field, while oxygen anions are still immobile due to their low mobility. If we neglect carrier diffusion, then the  $\text{Na}^+$  charge content inside the glass is a stepwise profile, which travels towards the cathode with an instantaneous speed  $v(t)$ .

Referring to Fig. (1), denoting by  $J_+$  the normalized charge flux of the sodium cations, the depletion layer front  $\Gamma$  is displaced by an amount  $dx$  during the time interval  $dt$  such that

$$dx = J_+ \cdot dt \quad (1)$$

Note that the glass-metal interface at  $x=0$  is not a source of sodium ions, and therefore  $J_+ = 0$  for  $0 \leq x \leq \Gamma$ . The electric field build-up in the depletion layer follows Gauss-Poisson law:

$$\frac{\partial E}{\partial x} = \rho / \varepsilon \quad (2)$$

, where  $\varepsilon$  is the dielectric constant of the depletion layer medium. Outside the depletion region, the electric field is uniform. Assuming that the entire potential drop occurs within the glass thickness  $L$ , the electric field profile must satisfy

$$V_0 = \int_0^L E dx \quad (3)$$

, where  $V_0$  is the applied voltage.

The local charge flux relates to the local electric field value and local charge densities according to a constitutive relationship  $J = J(E, \rho)$  that is usually written in the form

$$J_+ = \mu_+ \cdot \rho_+ \cdot f(E) \quad (4)$$

, where  $\mu$  is the ion mobility. In the absence of oxygen transport, Eqs. (1) to (4) determine the time evolution of the depletion layer,  $\Gamma(t)$ . The simple case of ohmic behavior for  $\text{Na}^+$  transport,  $J_+ = \mu_+ \cdot \rho_+ \cdot E$ , yields the same solution that Albaugh (1991) found through a variable-capacitance equivalent circuit model. Note that, as the depletion layer front advances, the local electric field increases at the glass-metal interface and decreases in the layer front; therefore, the speed of advance  $v(t)$  decreases in time.

Now if one considers the actual sodium content of commercial glasses suitable for anodic bonding, it can be shown that sodium drift inside the glass cannot proceed for long times without charge compensation. With  $\text{Na}^+$  transport alone, the electric field around the glass-metal interface would quickly reach values well above the glass dielectric strength (Rios et al., 2000).

Inclusion of anion transport is done by a continuity equation for the oxygen charge density

$$\frac{\partial \rho_-}{\partial t} = - \frac{\partial J_-}{\partial x} \quad (5)$$

and by a corresponding constitutive relationship

$$J_- = \mu_- \cdot \rho_- \cdot f(E) \quad (6)$$

Qualitatively, as the electric field values in the depletion layer get higher, the counter-flux of oxygen anions towards the glass-metal interface becomes appreciable. We then expect that an essentially charge-neutral region in the depletion layer develops with time, which limits the value of the electric field at the glass-metal interface. Fig. (1) shows typical profiles for charge densities and electric field that are expected during the depletion layer build-up.

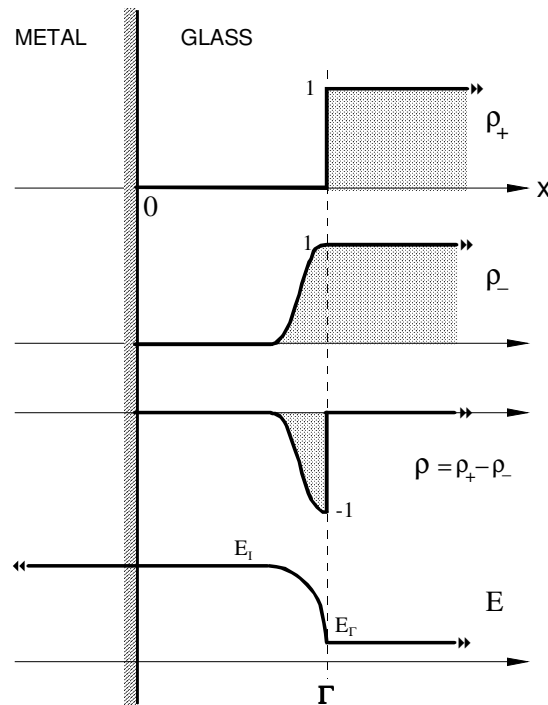


Figure 1 – Typical charge profiles and electric field during development of the depletion layer, with both sodium (+) and oxygen(-) ion transport.

### 3. NUMERICAL SCHEME

The numerical strategy takes into account that (1) oxygen transport inside the glass is negligible outside the depletion layer, where the electric field is uniform and steady decreasing in time; (2) the depletion layer front speed decreases in time, and (3) a stable numerical scheme is needed for the time integration of Eq. (5).

Neglecting the oxygen transport outside the depletion layer is also justified from the point of view that, for  $x > \Gamma$ , even in the presence of sodium drift, oxygen atoms remain essentially bounded to  $\text{Na}_2\text{O}$  ionic pairs; with that in mind, we actually impose a null-flux of  $\text{O}^-$  when the local  $\text{Na}^+$  charge density is unperturbed.

Finite-difference discretization is done using fixed time-steps  $\Delta t$ . Eqs. (1) to (6) is then treated as a moving boundary problem, which is integrated according to the following algorithm:

1. from the current value of the electric field at  $\Gamma$ , obtain the local flux of the  $\text{Na}^+$  cations from the constitutive relation, Eq. (4);
2. calculate the displacement  $\Delta x$  of the depletion-layer front during the time-interval  $\Delta t$ , according to Eq. (1);

3. from the current values of the electric field inside the depletion-layer region and the anion charge density profile  $\rho_-(x)$ , obtain the local flux of the oxygen anions at the current time, using the constitutive relation, Eq. (6);
4. obtain the charge density profile  $\rho_-(x)$  at time  $t+\Delta t$  by a Crank-Nicholson semi-implicit integration of the continuity equation, Eq. (5);
5. from the net charge field  $\rho = \rho_+ - \rho_-$ , the electric field at time  $t+\Delta t$  is found by integration of the Poisson Eq. (2) subjected to the normalization of the total potential, Eq. (3).

Initial conditions (when  $t=0$  and  $\Gamma=0$ ) are  $E = E_0 = V_0/L$ ,  $\rho_+ = \rho_- = 1.0$  (uniform fields). Note that, as time goes on, step 2 establishes a variable space mesh over the domain  $0 \leq x \leq \Gamma$ .

### 3.1 Details of the variable-mesh finite-difference Crank-Nicholson scheme

In the following,  $A_i^0$  and  $A_i$  stands for the value of the field  $A$  at mesh position  $i$  at times  $(t)$  and  $(t+\Delta t)$ , respectively, while  $\bar{\rho}_i^0$  and  $\bar{\rho}_i$  are values at  $(t)$  and  $(t+\Delta t)$  of the charge density value over the mesh interval  $(i, i+1)$ . In this section,  $\rho$  and  $J$  refer to the anion charge density and flux; we omit the charge label "-" for clarity.

Discretization of the continuity equation for the oxygen anions is done inserting the constitutive relation Eq. (6) into Eq. (5) and adopting a semi-implicit approximation for the charge density:

$$J_i = \frac{\rho_i^0 + \rho_i}{2} \cdot \mu_i^0 \cdot f(E_i^0) \quad (7)$$

Electric field and local mobility values are treated explicitly in time.

Values of the electric field and charge fluxes are specified at mesh nodes, while charge densities are given stepwise at the mesh intervals. We number the mesh nodes as  $i=1(1)(M+1)$ , such that  $x_1=0$  and  $x_{M+1}=\Gamma$ . For the charge density at the nodes, we adopt a simple linear interpolation:

$$\rho_i = \frac{\bar{\rho}_{i-1} + \bar{\rho}_i}{2} \quad (8)$$

, with boundary conditions  $\rho_1 = \bar{\rho}_1$  and  $\rho_M = 1.0$ .

In that manner, we arrive at a simple tridiagonal system of algebraic equations for  $\bar{\rho}_i$ ,  $i=1(1)M$ , to be solved at each time-step.

### 3.2 Space mesh renormalization

As the mesh size  $M$  increases and the current mesh interval  $\Delta x$  at  $\Gamma$  decreases in time, a renormalization of the spatial mesh is done periodically after a fixed number of time-steps, thus preserving CPU time by avoiding a too-high spatial resolution far from the depletion-layer advancing front (where the charge field is likely to be nearly uniform).

The strategy is to merge two adjacent mesh intervals when the charge field gradient is smaller than a given threshold. This is done numerically by comparing the weighted numerical dispersion between two adjacent interval values of the charge density with a given minimum.

#### 4. NUMERICAL RESULTS

Values for the observed external electric current are proportional to the sodium cations flux, which is evaluated from Eq. (4) at the interface position  $\Gamma$ . In the simple linear (ohmic) model,  $J_+$  has the same behavior of the local electric field at  $\Gamma$ . Numeric results are shown in Fig. (2), using reasonable known estimates for the physical constants, and the same experimental settings used by Albaugh, 1991 (anodic bonding of Silicon to Pyrex glass). Those are listed in Table 1.

Table 1. Dimensional values of parameters employed in the numeric simulations

	<i>Parameter</i>	<i>Symbol</i>	<i>Value</i>
<i>Experimental settings</i>	Applied voltage	$V_0$	1000V
	Glass thickness	$L$	3,2mm
<i>Physical properties</i>	Dielectric constant	$\epsilon$	$7\epsilon_0$
	Permittivity of free space	$\epsilon_0$	$8.85 \times 10^{-12}$ F/m
	Sodium charge content	$n_{0+}$	$2.77 \times 10^8$ C/m <sup>3</sup>
	Ionic resistivity of Na <sup>+</sup>	$r$	$1.1 \times 10^5$ $\Omega$ .m

Characteristic values of length  $l_D$  and time  $\tau$  for the depletion zone dynamics can be defined as

$$\left\{ \begin{array}{l} l_D = \sqrt{\frac{2\epsilon V_0}{n_{0+}}} \\ \tau = \frac{2\epsilon r L}{l_D} \end{array} \right. \quad (9a)$$

$$\left\{ \begin{array}{l} \tau = \frac{2\epsilon r L}{l_D} \end{array} \right. \quad (9b)$$

, and they are  $l_D = 2.12 \times 10^{-8}$  m ;  $\tau = 2.06$  s for the settings of Table 1.

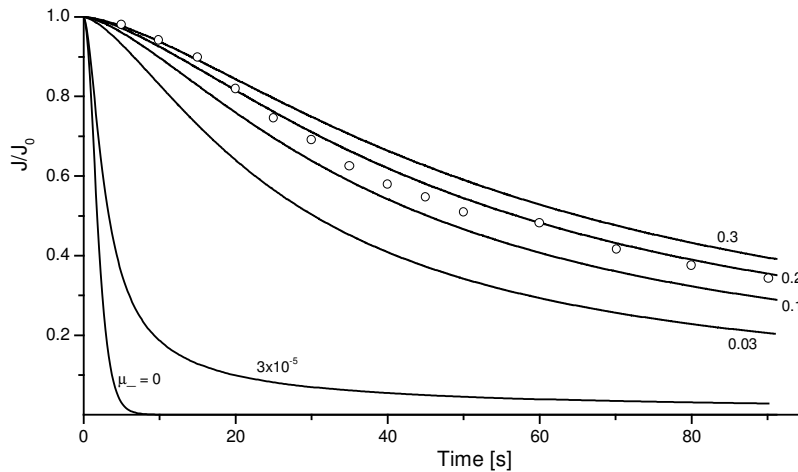


Figure 2 – Decay of the normalized electric current in time, as a function of the oxygen anion mobility  $\mu_-$ . Open circles are experimental points measured by Albaugh (1991). Solid curves are the results of the numeric simulations. The mobility of cations is held fixed at the value  $\mu_+ = 1$ .

The numeric results shown in Fig. (2) for  $\mu_- = 0$  was obtained by Albaugh (1991) with an equivalent circuit model. There is a fair general agreement between our model and the observed behavior of the electric current decay, both for short and long time regimes, as far as the oxygen mobility in the glass reaches  $\sim 20\%$  of the sodium mobility. In that case, most of the depletion layer is almost neutral and uniform, the net charge profile resembling a delta function around  $\Gamma$  (Fig. 3).

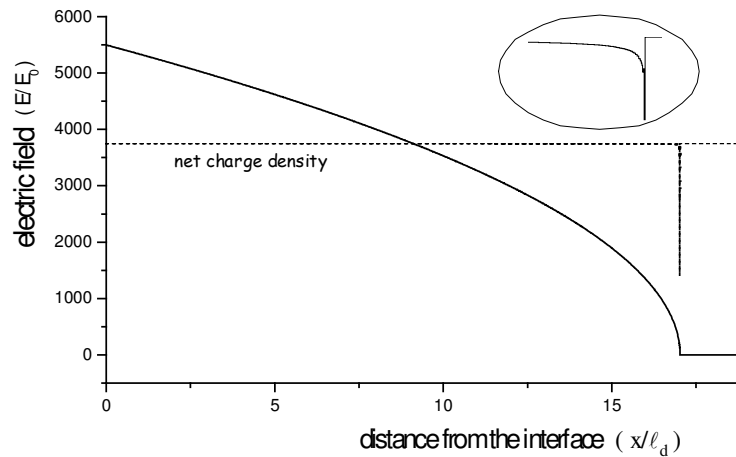


Figure 3 – Electric field and net charge profile in the depletion zone for  $\mu_- = 0.2$ , at time  $21.4\tau$  (44.1s). The inset is an enlargement of the net charge profile around the depletion layer front  $\Gamma$ .

Values of the computed depletion layer width can be seen in Fig. (4). Depletion lengths are dramatically increased for high anion mobility, and that is in accordance with the experimental results of Wallis (1970), that reported depletion widths of the order  $500\ell_D$ .

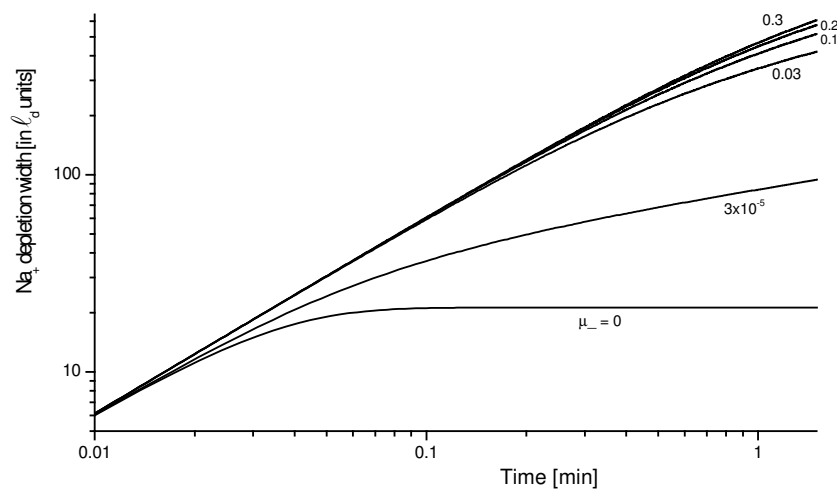


Figure 4 – The computed depletion layer advance in time, as a function of the oxygen anion mobility  $\mu_-$ .

The electric field at the silicon-glass interface attains lower values, more compatible with the dielectric strength of pure silica ( $\sim 10^7$  V/cm), as the anion mobility increases. This is shown in Fig. (5).

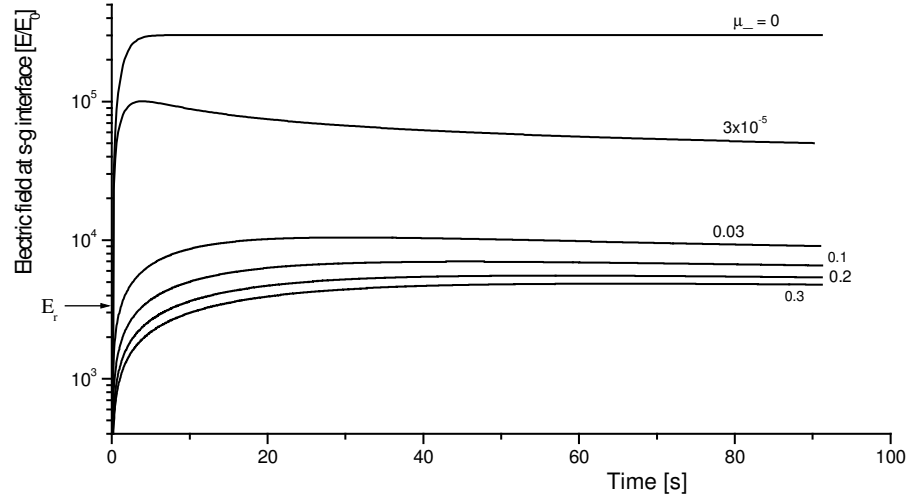


Figure 5 – Numerical results for the electric field at the silicon-glass (s-g) interface during the anodic transient, as a function of the oxygen anion mobility  $\mu_-$ .  $E_r$  is the rupture field in pure silica.

## 5. EFFECTS OF THE OXIDE LAYER GROWTH

Deposition of oxygen at the anode results in a continuous growth of an insulating oxide layer at the metal-glass interface, of thickness  $x_0(t)$ . In the numeric simulations, that can be taken into account by considering an uniform electric field in the layer region,  $-x_0 \leq x \leq 0$ , and modifying Eq. (3) as

$$V_0 = \int_{-x_0}^L E dx \quad (10)$$

The detailed growth dynamics of the oxide layer should consider that oxygen atoms coming from the glass accumulate at the glass-metal interface and only reach metal atoms through diffusion across the layer  $x_0$ . As a first simplified model, we here consider that oxygen atoms are instantaneously incorporated into the metal matrix to form an uniform oxide layer. In that case, the increase  $dx$  of the oxide layer during the time interval  $dt$  can be found from the anion flux  $J_-$  at the metal-glass interface ( $x=0$ ) and the value of the oxygen charge density in the oxide,  $n_{ox}$ :

$$dx = \frac{dt}{n_{ox}} J_-(0,t) \quad (11)$$

Inclusion of Eqs. (10) and (11) in the numeric model is straightforward. Calculations were done for a silicon-glass interface. Each molecule of silicon oxide,  $\text{SiO}_2$ , carries two oxygen anions, which correspond to four elementary charges. From the known molecular density  $n_{\text{SiO}_2} = 2,3 \times 10^{22}$  molecules/ $\text{m}^3$  (Ruska, 1987), we thus have  $n_{\text{ox}} = 1.5 \times 10^{10}$  C/ $\text{m}^3$ .

On the assumption that, in the glass, the only source of oxygen atoms is the dissociation of  $\text{Na}_2\text{O}$ , using the known data for the sodium content in Pyrex glass (Albaugh, 1991) gives a rough estimate

$$18 \leq \frac{n_{\text{ox}}}{n_{0+}} \leq 60 \quad (12)$$

Fig. (6) shows results of the numeric simulations with our simplified homogeneous oxide layer growth. Unfortunately, it seems that consideration of the potential drop through the oxide layer does not improve the qualitative agreement between the model and the experimental data.

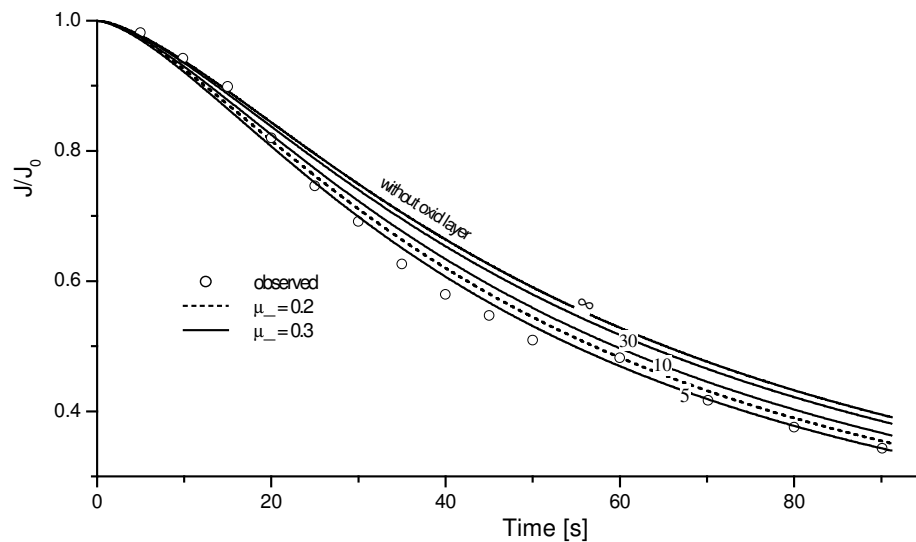


Figure 6 – Numerical estimate of the influence of the oxide layer growth at the silicon-glass interface on the measured electric current transient. That is to be compared to Fig. (2). The numbers that label the curves are the values for the normalized oxygen charge density in the oxide, Eq. (12).

## 6. CONCLUSIONS AND COMMENTS

The numeric simulations point towards the importance of anion transport in the glass even at very early times during electrostatic silicon-glass (s-g) bonding process. High oxygen mobility in the glass limits the electric field to moderated values at the s-g interface and provided for large depletion layer widths. Those findings are in accordance to the known experimental data, as far as electric transients are concerned.

Experimental data from Albaugh (1991) seems to indicate that a large electric current is sustained for long times (an order of magnitude greater than the characteristic depletion time) at initial stages of the process. Our model, with the current assumptions cannot explain that. Inclusion of an additional potential drop due to oxide growth at the s-g interface does not improve qualitatively the numeric predictions. Further experimental data under controlled conditions are thus desirable, and are being devised at our facilities at INPE.

Computations were done in a 2GHz Asus-Athlon PC machine with the gcc compiler. Stability of the adopted Crank-Nicholson semi-implicit scheme requires smaller values for the time-step  $\Delta t$  as the anion mobility  $\mu_-$  increases. As a typical example, integration for  $\mu_- = 0.2$  ( $\tau=2.06$ ) during the first 90 seconds of the depletion layer growth required a maximum time-step of  $1.5 \times 10^{-5} \tau$  and takes nearly an hour and a half of CPU time.

The model here described is suitable to encompass a whole class of mobility and cross-ionic transport models. Improvements can be made both in the fixed-time integration strategy and mesh renormalization, towards a truly adaptive algorithm. In the present form, excessive CPU time is required as the ratio of anion to cation mobilities approach 1.0 .

## REFERENCES

- Anthony, T.R., 1983. Anodic bonding of imperfect surfaces. *J. Appl. Phys.* **54**, pp.2419-2428.
- Albaugh, K.B., 1991. Electrode Phenomena during Anodic Bonding of Silicon to Sodium Borosilicate Glass *J. Electrochem. Soc.* **138**, pp.3089-3094.
- Carlson, D.E.; Hang, K.W. and Stockdale, F., 1972. Electrode Polarization in Alkali-containing Glasses *J. Am. Cer. Soc.* **55**, pp.337.
- Rios, A.N.; Gracias, A.C.; Maia, I.A. and Senna, J.R., 2000. Modeling the Anodic Current in Silicon-Glass Bonding. *Rev. Bras. Aplic. Vacuo* **19**, pp.31-34.
- Ruska, W.S., 1987. Microelectronic Processing. McGraw-Hill.
- Wallis, G. and Pomeranz, D.I., 1969. Field Assisted Glass-Metal Sealing *J. Appl. Phys.* **40**, pp.3946.
- Wallis, G., 1970. Direct-Current Polarization during Field-Assisted Glass-Metal Sealing. *J. Am. Cer. Soc.* **53**, pp.563.